DOI: 10.1002/anie.200((will be filled in by the editorial staff))

Steady-State Continuous-Flow Purification by Electrophoresis**

*Fletcher J. Agostino, Leonid T. Cherney, Victor Galievsky, and Sergey N. Krylov**

Continuous-flow microsynthesis has a number of important advantages over batch synthesis, namely: increased product yield through atom economy,[1-3] reduced costs associated with starting materials,[4] safer operating conditions,[5,6] high-throughput production by numbering up,[7-9] and automated optimization and control of reaction conditions.[10,11] To fully exploit these advantages, continuous-flow microsynthesis should be followed by continuous-flow purification in a compatible scale. Such a combination has not yet been practically realized due to a lack of a suitable purification technique.[12] Continuous-flow purification can be achieved if a continuous-flow microreactor exits into a wide purification channel in which products are separated in the direction orthogonal to the flow and continuously collected at the exit of the channel. Our recent research efforts have been motivated by understanding that an existing continuous-flow purification technique, free flow electrophoresis (FFE), is naturally suited for combination with continuous-flow microsynthesis in aqueous solution (**Fig. 1a**).

FFE facilitates continuous separation of molecules in a wide separation channel with a uniform hydrodynamic flow of an electrolyte solution and an electrical field non-parallel (typically orthogonal) to this flow.[13,14] The sample is introduced into the separation channel through a narrow opening as schematically shown in **Fig. 1a**. Advantageously, FFE devices can be made in a small scale to suit small flow rates used in continuous-flow microsynthesis.[15] Unfortunately, small-scale FFE cannot be used for steady-state purification.[16] Electrolysis of water leads to the formation of O_2 and H_2 bubbles on the surface of the electrodes. Bubble accumulation on the electrodes and subsequently in other parts of the device leads to progressing electric field distortion and diminishing quality of purification within the first several minutes of operation.[17,18] The regeneration of an FFE device requires complete bubble flush-out: a cumbersome and time-consuming process. The goal of this work was to find an ultimate solution for the problem of FFE instability caused by bubble accumulation, thereby permitting reliable steady-state operation without the distortion of electric field or separation quality. Solving the bubble-accumulation problem is pivotal to FFE integration with other micro-systems.[19]

The previous approaches to the problem of bubble accumulation in FFE devices could be split into three major categories: (i) mechanical barrier preventing the entry of bubbles into the separation channel,[20] (ii) separate electrode channels with fast flow for bubble removal,[21] and (iii) chemical agents that inhibit gas generation and bubble growth.[22] While being useful, these measures only delay the accumulation of the deteriorating amount of bubbles. Bubbles still accumulate and prevent steady-state continuous separation. Because of bubble accumulation, electrical-current and sample-flow stability in FFE typically lasts for less than 0.5 h.[22] The longest demonstrated operational time for small-scale FFE is 2 h.[23]

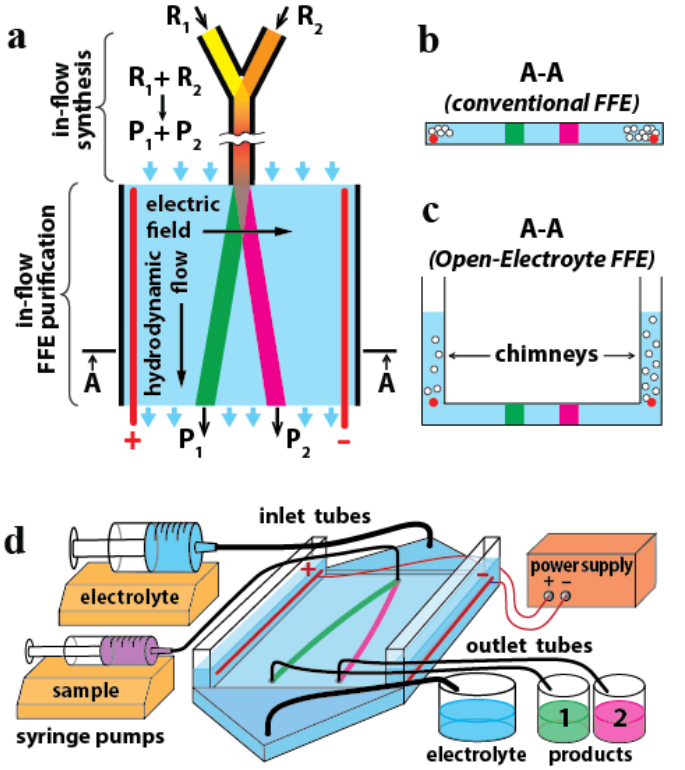

Figure 1. (**a**) Schematic top view of an integrated system for continuous-flow microsynthesis followed by continuous-flow purification. The reactants, R_1 and R_2, generate products, P_1 and P_2, which are separated by FFE. A conceptual comparison of cross-sections (section A-A in panel (**a**)) in devices for conventional FFE (**b**) and our OEFFE (**c**). In OEFFE, bubbles (o) generated at the electrodes (●) are vented out of the device into the atmosphere through the chimneys. (**d**) General overview of an OEFFE device.

This work was inspired by an insight that an ultimate solution to the bubble-accumulation problem could be achieved by breaking a paradigm of a closed FFE device. Our logic was simple. Bubble removal into the atmosphere could be easy and natural if the electrolyte above the electrodes was open to the atmosphere. Further, engineering the "open-concept" FFE device requires vertical chimneys to hold a column of electrolyte that hydrostatically balances the pressure inside the device. Since the Archimedes force pushes the gas upwards, bubble entry into the separation channel can be completely prevented by placing the electrodes in the chimneys above the level of the separation channel. We term this approach Open-Electrolyte FFE (OEFFE). **Figure 1** schematically illustrates the differences between the classical planar FFE device (**b**) and an OEFFE device with chimneys (**c**). Ideally, the setup should be designed to include a way to collect sample fractions after being purified, and also to collect and potentially recycle the electrolyte. The general schematic of an OEFFE device is illustrated in **Fig. 1d**, and a detailed drawing is shown in **Fig. S1**.

[*] F.J. Agostino, Dr. L.T. Cherney, Dr. V.Galievsky, Prof. S.N. Krylov
Department of Chemistry and Centre for Research on Biomolecular Interactions, York University
4700 Keele Street, Toronto, Ontario M3J 1P3, Canada
Fax: (+) 416-736-5936, E-mail: skrylov@yorku.ca

[**] We thank Natural Sciences and Engineering Research Council of Canada.

Supporting information for this article is available on the WWW under http://www.angewandte.org or from the authors

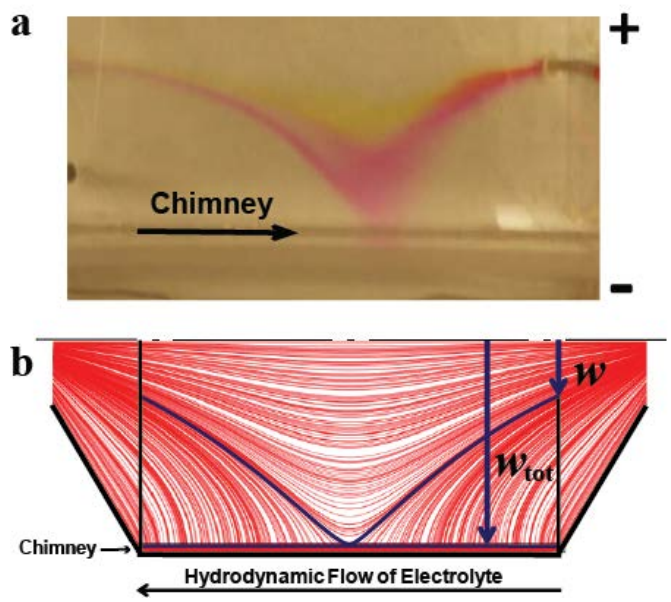

Figure 2. Flow non-uniformity in non-optimized OEFFE device: **(a)** real and **(b)** virtual. The hydrodynamic flow rate in both the virtual and real devices was 5 mL/min. A mixture of 2 dyes (fluorescein and rhodamine B) was continuously injected in the real device at a rate of 4 μL/min. The electric field was 50.0 V/cm. In the non-optimized device, the dye streams were deflected into the chimneys, diminishing the quality of separation. The virtual model illustrates the definition of the optimization parameter w/w_{tot} (see details in the text). Maximizing this parameter leads to a more uniform flow across the width of the separation channel. The value of w/w_{tot} in this example is 0.26 while its theoretical maximum is 1. All parts show halves of the devices.

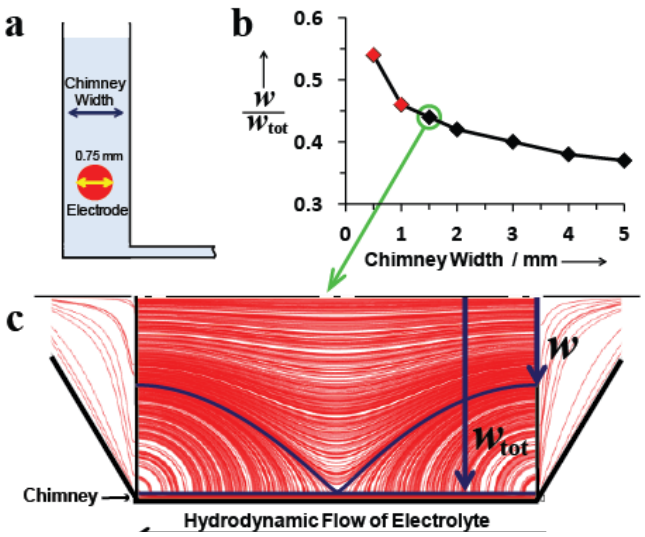

Figure 3. *In*-silico optimization of flow uniformity based on chimney width. **(a)** Schematic of the chimney, highlighting the chimney width in relation to the electrode width. **(b)** Dependence of flow uniformity on the width of the chimney, where (♦) identifies chimney widths that are unfeasible because of the electrode diameter being a physical limitation. **(c)** *In-silico* product of optimizing the flow by decreasing the chimney width to 1.5 mm. The resultant w/w_{tot} is equal to 0.44.

We first attempted to test OEFFE experimentally by adding the chimneys to the previously developed and optimized planar device.[24] The parts of the device were made of poly(methyl methacrylate) by robotic micro-milling and bonded together with dichloromethane. Despite the apparent simplicity of OEFFE, all of our initial attempts to construct a functional OEFFE device had failed. The flow through the separation channel was not uniform (streamlines were significantly curved) and always diverted from the separation channel into the chimneys (**Fig. 2a**). Experimental variation of the device geometry and operation conditions proved to be a slow and inefficient way of solving this problem.

Difficulties of experimental optimization of a real OEFFE device prompted us to design a virtual OEFFE device for its *in-silico* optimization before manufacturing a real device. The virtual OEFFE device was constructed with COMSOL Multiphysics 4.3a commercial software (COMSOL Group, Palo Alto, CA), a program which allows complete modeling of the flows within the device. The COMSOL simulation uses 3D modeling and presents the streamline patterns from a top-view for clarity of demonstration. The Experimental Section highlights experimental parameters, equations, meshing conditions, and boundary conditions used. To reduce computation time, we simulated a half of the symmetrical device (**Fig. S2** shows simulation of the full device).

We studied a number of virtual devices mimicking the initial experimental devices which had non-uniform flows. The flows in the virtual devices were similar to the ones in the real devices (see example in **Fig. 2**), which proved the accuracy of the virtual device operation. After this test, we could use the virtual OEFFE device for the optimization of its geometry. The goal was to achieve as uniform flow in the separation channel as possible. A numerical parameter used to characterize flow uniformity was a ratio w/w_{tot} (see **Fig 2b**). Here, w is the width of the part of the separation channel entry gate which incorporates only streamlines that do not leave the main part of the separation channel and w_{tot} is the total width of the entry gate that does not include chimneys. A greater value of w/w_{tot} corresponds to a more uniform flow, and, thus, optimization was done through maximizing w/w_{tot}.

Our optimization procedure required the identification of geometric parameters that could be varied to maximize w/w_{tot}. It is already known that the correct geometry of triangular electrolyte-entrance and electrolyte-exit reservoirs (located, respectively, at the top and bottom of an FFE device, see **Fig. S1**) are essential for establishing parallel flow streamlines through a small-scale FFE device without chimneys.[24] The separation channel thickness was set to 200 μm, which was the minimum value to achieve reproducible FFE results using our fabrication technique.[25] In such a case, the movement of a viscous fluid in a shallow separation channel is possible when a pressure difference is applied between the input and output, i.e. there is a pressure gradient along the flow. However, in OEFFE, the introduction of chimneys, which are open to the atmosphere, provide isobaric pressure along the entire boundary with the separation channel. Thus, there exists strong pressure non-uniformity at the boundary, and, as a result, undesirable fluid transferring occurs between the separation channel and chimneys.

We first attempted to optimize the chimney width, (**Fig. 3a**) and our simulations showed that decreasing the width of the chimneys increases w/w_{tot} to a value of 0.54 when the chimney is 0.5 mm wide (**Fig. 3b**). Our limitation, however, is that the chimney width cannot be smaller than the diameter of the electrode (0.75 mm) and in reality should allow extra space for bubble escape. We, therefore, set the minimum chimney width to 1.5 mm ($w/w_{tot} = 0.44$). This width is not sufficiently small to achieve a uniform flow (**Fig. 3c**).

To further optimize flow uniformity we needed a new feature in the device that could significantly decrease the undesirable pressure gradient across the separation channel. We suggested that deep and narrow sacrificial channels, parallel to the separation channel and located between the separation channel and the chimneys, could help to solve the problem (**Fig. 4a**). Explaining the design and implementation of sacrificial channels follows this logic. The sacrificial channel has a much larger volumetric flow rate than the separation channel, because of its greater depth, and as a result the flow within it is less likely to diverge into the chimneys.

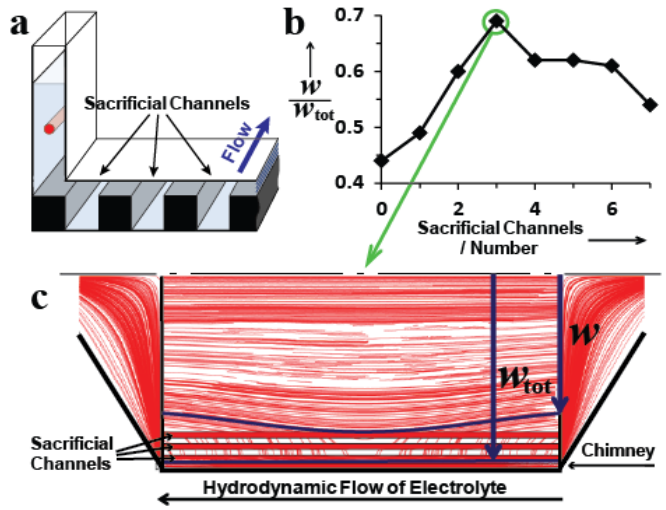

Figure 4. *In-silico* optimization of hydrodynamic flow uniformity with respect to the number of sacrificial channels. (**a**) Schematic of sacrificial channels built into the separation channel. (**b**) Dependence of uniform flow on the number of sacrificial channels constructed in the separation channel. The optimal number of sacrificial channels is 3, with a $w/w_{tot} = 0.69$. (**c**) Improvement in flow uniformity after 3 sacrificial channels are introduced.

Additionally, the influence of the isobaric boundaries in the chimneys on the fluid dynamics in the separation channel can be further reduced. We decided to explore the use of multiple parallel sacrificial channels, separated by narrow spaces, which could attenuate the fluid exchange between adjacent sacrificial channels (**Fig. S3**). As a result, we thought that sacrificial channels could prevent the flow divergence towards the chimneys.

We first introduced a single sacrificial channel and found that our hypothesis was correct - it improved flow uniformity. We then optimized its width and depth (**Fig. S4**). As a result, we limited both the width and depth of the sacrificial channel to 1.5 mm which generated a marginal increase in the value of w/w_{tot} from 0.44 to 0.49. In an attempt to further improve flow uniformity, we explored the effect of multiple sacrificial channels. To facilitate the faster optimization process we assumed that: (i) all sacrificial channel have the same dimensions and (ii) the distances between them are equal. We discovered that the dependence of w/w_{tot} on the number of sacrificial channels displays a maximum when the number of channels was equal to 3 (**Fig. 4b**). Three sacrificial channels allowed us to achieve $w/w_{tot} = 0.69$ (**Fig. 4c**). While the width of the sacrificial channel was an important optimization parameter (**Fig. S4b**), one wide channel did not have the same effect as 3 narrow channels (**Fig. S5**). We also tested our final *in-silico* product for its robustness with respect to separation channel depth (**Fig. S6**) and hydrodynamic flow rates (**Fig. S7**). These simulations were performed to ensure that any variability that might be caused by machining or operational precision did not significantly affect the device performance. In both cases, the optimized OEFFE proved to be robust.

The hard copy of the *in-silico*-optimized OEFFE device was then manufactured using the approach described above. The device was first tested for flow uniformity. The sample flow had relatively straight streamlines suggesting that the optimization was successful, and once again proving the accuracy of the virtual device operation. We then tested the device for bubble formation. Bubbles formed on the electrodes and dislodged from them when they reached the critical size. Bubbles vented out into the atmosphere and did not enter the separation channel. Under such conditions the electric current showed no drift during a 12-h period of continuous work, thus, suggesting its steady-state bubble removal.

Our final test was for stability of electrophoretic separation. A mixture of three dyes (rhodamine B, rhodamine 6G, and fluorescein) was continuously injected by a syringe pump that provided uninterrupted injection for 12 h. The stability of separation was judged by the steadiness of the 3 streamlines. No deterioration in separation quality was noticed (**Fig. 5**), suggesting the steady-state operation of the device. On the other hand, only negligible widening of streamlines during their passage through the separation channel suggests minimal contribution from multiple sources of band-broadening such as diffusion, injection bandwidth, convection, and hydrodynamic broadening. Injection bandwidth is limited by simply decreasing the diameter of the sample inlet. Decreasing the depth of the separation channel reduces convective and hydrodynamic broadening.[19] Therefore, not only can this device support steady-state continuous separation, but it also satisfies the general requirement of negligible band broadening.

To conclude, we have successfully demonstrated steady-state small-scale continuous separation. OEFFE ultimately solves the problem of the deterioration of separation quality over time by preventing the accumulation of bubbles in the device. The introduction of chimneys caused non-uniformity in hydrodynamic flow, which was circumvented by novel features called sacrificial

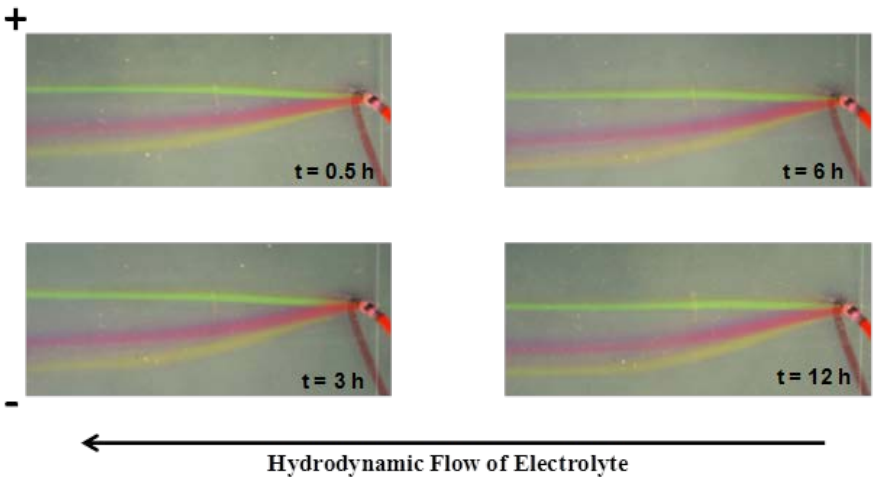

Figure 5. Steady-state continuous separation of 250 mM fluorescein (green), 250 mM rhodamine B (pink), and 250 mM rhodamine 6G (yellow) by OEFFE. An electric field of 50.0 V/cm was applied across the chip for a 12-h period. The hydrodynamic flow rate of the electrolyte was 5.00 ± 0.5 mL/min. A mixture of the three dyes was introduced at a flow rate of 4.00 ± 0.01 µL/min. Current reading was stable at 25 ± 1 mA. Removing the bubbles from the OEFFE device prevented electric field distortion and supported its steady-state separation with constant quality of separation.

channels. With the assistance of COMSOL simulations, we found the appropriate geometries of the chimneys and sacrificial channels to achieve acceptable flow uniformity. According to our results, flow uniformity can be further optimized and will be evaluated in future studies. Although we have only developed an OEFFE prototype in plastic, it will be prudent to create analogues in solvent resistant material, in order to expand the scope of solvents and analytes for which OEFFE is suitable. It should be noted that classical electrophoresis is applicable for separation of analytes with different charge/size ratios. Modifications of classical electrophoresis have been developed for the separation of uncharged species. Micellar electrokinetic chromatography uses charged surfactants, at concentrations that are greater than critical micelle concentration, to separate uncharged species with different hydrophobicities.[26-28] Dielectrophoresis, another example, uses non-uniform electric fields to separate uncharged species with different dipole moments.[29,30] Achieving steady-state continuous separation, with a technologically-simple solution, will stimulate efforts aiming at practical integration of continuous microsynthesis with continuous purification.

Experimental Section

To simulate OEFFE devices we used COMSOL. The steady state Navier-Stokes equation was used for the *in-silico* computations, with the condition of non-compressible flow. The laminar flow physics model was chosen and we input a flow rate of 5 mL/min into the electrolyte inlet (shown in **Fig. S1**). The boundary conditions include: no-slip walls; laminar inflow at the inlet; and no viscous stress at the outlet. The meshing geometry used was tetrahedral, with a fine size in areas of large volume (exit and entrance reservoirs), and extremely fine geometry in narrow regions (separation channel, sacrificial channels, and chimneys). Default stabilization conditions (with a tuning parameter $C_k = 1$) were selected: streamline diffusion and crosswind diffusion. 3-D models were prepared to fully capture the flow system in only one half of the device to facilitate simulation time. We have included in the Supporting Information the optimized COMSOL file thoroughly detailing our simulation strategy. The mathematical model includes the following relations. Laminar flow equations inside the device:

$$\rho(v \cdot \nabla)v = \nabla \cdot [-pI + \mu(\nabla v + \nabla v)^{\mathrm{T}})]$$
$$\rho \nabla \cdot v = 0$$

Wall boundary condition:

$$v = 0$$

Inlet condition:

$$L_{\mathrm{entr}} \nabla_t \cdot [-p_{\mathrm{entr}} I + \mu(\nabla_t v + \nabla_t v)^T] = -p_{\mathrm{entr}} n$$
$$\nabla_t \cdot v = 0$$

Outlet condition:

$$p = p_0, \qquad [\mu(\nabla v + (\nabla v)^T] \cdot n = 0$$

Symmetry conditions at the symmetry plane $x = 0$:

$$v \cdot n = 0, \qquad K - (K \cdot n)n = 0$$
$$K = [\mu(\nabla v + (\nabla v)^T]n$$

Here, ρ and μ are density and viscosity of the liquid; v and p are the velocity and pressure; K is the viscous force at the symmetry plane; p_{enter} and p_0 are the pressures at the inlet and outlet, respectively; L_{entr} is a parameter used by COMSOL in the inlet condition, I is the unit tensor; n is the normal to the walls or to the symmetry plane; the superscript T denotes a transpose matrix.

All reagents were purchased from Sigma Aldrich, unless otherwise mentioned. OEFFE prototypes were fabricated from poly(methyl methacrylate) stock material using a MDX-540 robotic milling machine. The optimized cutting speeds for the end mills have already been described in full detail.[24] Refer to Supporting Information (Experimental Details) for full details of OEFFE assembly.

An electrolyte solution was prepared with 25 mM 4-(2-hydroxyethyl)-1-piperazineethanesulfonic acid (HEPES) (99.5%) and was adjusted with 10 M NaOH to pH 7.5. Triton X-100 (0.001 [w/v]) was added to it and the mixture was deoxygenated by bubbling with N_2 overnight. A sample containing 250 mM of each fluorescein, rhodamine B, and rhodamine 6G, was prepared in this electrolyte. A separate 10% EtOH solution was used as a primary wash solution to wet the surface of the OEFFE device. All solutions were prepared using de-ionized H_2O.

The hydrodynamic flow of the electrolyte was driven by a continuous flow syringe pump system (New Era Pump System Inc, Farmingdale, NY, USA). The electrolyte flow rate in the experiment highlighted in the paper was 5.00 ± 0.05 mL/min. A separate syringe pump (Harvard Apparatus Pump II, Saint-Laurent, Canada) was used to introduce the sample at a flow rate of 4.00 ± 0.01 µL/min. Experiments were carried out at room temperature. The OEFFE device was placed on top of metal blocks, which were in contact with ice packs, to help prevent overheating.

The voltage applied to the electrodes was 500 V, which correcponds to an electric field strength of 50.0 V/cm inside the separation channel. For 12 hours, the current was recorded and digital pictures (Nikon 7000) were taken to monitor the sample separation quality in the presence of an electric field.

Received: ((will be filled in by the editorial staff))
Published online on ((will be filled in by the editorial staff))

Keywords: free-flow electrophoresis · bubbles · continuous flow microsynthesis · COMSOL · open-electrolyte

(1) Burns, J. R.; Ramshaw, C. *Chem. Eng. Res. Des.* **1999**, *77*, 206-211.
(2) Wiles, C.; Watts, P.; Haswell, S. J.; Pombo-Villar, E. *Tetrahedron* 2005, *61*, 10757-10773.
(3) Chambers, R. D.; Fox, M. A.; Sandford, G. *Lab Chip* **2005**, *5*, 1132-1139.
(4) Comer, E.; Organ, M. G. *J. Am. Chem. Soc.* **2005**, *127*, 8160-8167.
(5) Wada, Y.; Schmidt, M. A.; Jensen, K. F. *Ind. Eng. Chem. Res.* **2006**, *45*, 8036-8042.
(6) Kockmann, N.; Roberge, D. M. *Chem. Eng. Technol.* **2009**, *32*, 1682-1694.
(7) Schenk, R.; Hessel, V.; Hofmann, C.; Kiss, J.; Löwe, H.; Ziogas, A. *Chem. Eng. J.* **2004**, *101*, 421-429.
(8) Ullah, F.; Samarakoon, T.; Rolfe, A.; Kurtz, R. D.; Hanson, P. R.; Organ, M. G. *Chem. – Eur. J.* **2010**, *16*, 10959-10962.
(9) Okafor, O. C.; Tadepalli, S.; Tampy, G.; Lawal, A. *Ind. Eng. Chem. Res.* **2010**, *49*, 5549-5560.
(10) Leung, S.-A.; Winkle, R. F.; Wootton, R. C. R.; deMello, A. J. *Analyst* **2005**, *130*, 46-51.
(11) Hatakeyama, T.; Chen, D. L.; Ismagilov, R. F. *J. Am. Chem. Soc.* **2006**, *128*, 2518-2519.
(12) Wiles, C.; Watts, P. *Eur. J. Org. Chem.* **2008**, 1655-1671.
(13) Hannig, K.; Wirth, H.; Meyer, B.-H.; Zeiller, K. *H.-S. Z. Physiol. Chem.* **1975**, 1209-1223.
(14) Hannig, K.; Wirth, H.; Schindler, R. K.; Spiegel, K. *H.-S. Z. Physiol. Chem.* **1977**, *358*, 753-764.
(15) Raymond, D. E.; Manz, A.; Widmer, H. M. *Anal. Chem.* **1994**, *66*, 2858-2865.
(16) Persat, A.; Suss, M. E.; Santiago, J. G. *Lab Chip* **2009**, *9*, 2454-2469.
(17) Revermann, T.; Gotz, S.; Kunnemeyer, J.; Karst, U. *Analyst* **2008**, *133*, 167-174.
(18) Vogt, H. *J. App. Electrochem.* **1983**, *13*, 87-88.
(19) Turgeon, R.; Bowser, M. *Anal. Bioanal. Chem.* **2009**, *394*, 187-198.
(20) Raymond, D. E.; Manz, A.; Widmer, H. M. *Anal. Chem.* **1996**, *68*, 2515-2522.
(21) Fonslow, B. R.; Barocas, V. H.; Bowser, M. T. *Anal. Chem.* 2006, *78*, 5369-5374.
(22) Kohlheyer, D.; Eijkel, J. C. T.; Schlautmann, S.; van den Berg, A.; Schasfoort, R. B. M. *Anal. Chem.* **2008**, *80*, 4111-4118.
(23) Frost, N.; Bowser, M. *Lab Chip* **2010**, *10*, 1231-1236.
(24) Fonslow, B. R.; Bowser, M. T. *Anal. Chem.* **2008**, *80*, 3182-3189.
(25) Agostino, F. J.; Evenhuis, C. J.; Krylov, S. N. *J. Sep. Sci.* **2011**, *34*, 556-564.
(26) Terabe, S.; Otsuka, K.; Ando, T. *Anal. Chem.* **1985**, *57*, 834-841.
(27) Terabe, S. *J. .Pharm. .Biomed. Anal.* **1992**, *10*, 705-715.
(28) Rizvi, S. A. A.; Do, D. P.; Saleh, A. M. *Eur. J. Chem.* **2011**, *2*, 276-281.
(29) Gascoyne, P. R. C.; Vykoukal, J. *Electrophoresis* **2002**, *23*, 1973–1983.
(30) Hughes, M. P. *Electrophoresis* **2002**, *23*, 2569-2582.

Entry for the Table of Contents

In-Flow Purification

Fletcher J. Agostino, Leonid T. Cherney, Victor Galievsky, and Sergey N. Krylov*

_____ **Page – Page**

Steady-State Continuous-Flow Purification by Electrophoresis

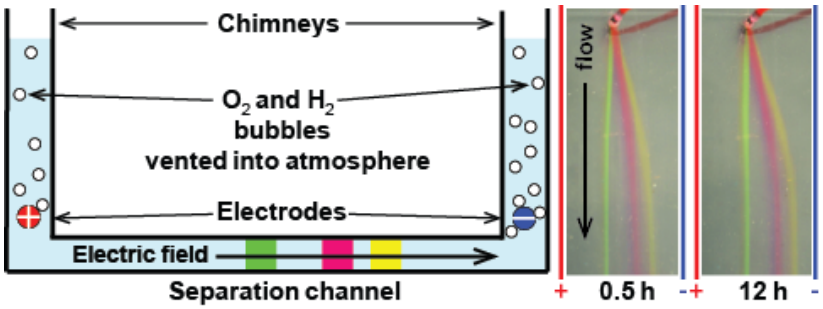

ABSTRACT: Free-flow electrophoresis (FFE) can potentially facilitate continuous-flow purification of products from continuous-flow microsynthesis. An arguably major limitation of FFE, in this application, is the short time of its uninterrupted stable operation. Gas bubbles, formed by the electrolysis of water, accumulate in FFE devices and distort the electric field and separation quality in a time scale of ~ 10 min to 1 h. Here, we propose an ultimate solution for the problem of gas accumulation in FFE devices. We introduce Open-Electrolyte FFE (OEFFE), in which the electrodes are placed in chimneys at a level higher than the separation channel, and the electrolyte in the chimneys is open to the atmosphere. The bubbles cannot enter the separation channel and are vented directly into the atmosphere. We constructed a working OEFFE prototype and demonstrated its absolutely stable operation over 12 h. OEFFE can thus support steady-state continuous purification. This result may be decisive in starting practical attempts to combine continuous-flow microsynthesis with continuous-flow purification.

SUPPORTING INFORMATION

Steady-State Continuous-Flow Purification by Electrophoresis

Fletcher J. Agostino, Leonid T. Cherney, Victor Galievsky, and Sergey N. Krylov

Experimental Details

All reagents were purchased from Sigma Aldrich, unless otherwise mentioned. OEFFE prototypes were fabricated using a MDX-540 robotic milling machine (Roland DGA, Irvine, CA). The stock material used was poly(methyl methacrylate) (PMMA) (Johnston Industrial Plastics, Toronto, Canada), and was cut using a series of end mill tools to accurately and precisely shape the prototypes. The optimized cutting speeds for the end mills have already been described in full detail (Agostino, F. J.; Evenhuis, C. J.; Krylov, S. N. *J. Sep. Sci.* **2011**, *34*, 556-564).

Fabrication of OEFFE involves milling bottom, top, and chimney substrates. The three substrates are then bonded together using small volumes of dichloromethane (CH_2Cl_2). CH_2Cl_2 was injected carefully to provide a tight seal at the edges of the device. The device was clamped together for 10 minutes to allow the solvent to completely perfuse and dry at the edges. Platinum electrodes (100 mm long and 0.75 mm in diameter) were installed into the chimneys and connected with insulated copper wires to a power source. The power source used was a high-voltage Electrophoresis Power Supply EPS 3501 XL (Amersham Pharmacia Biotech, New Jersey, USA). The completed device, with the appropriate dimensions, can be found in **Fig. S1**.

Metal Luer Stubs (of internal diameters depicted in **Fig. S1**) were used as fluidic adapters and polyethylene tubing was used to transfer the electrolyte and sample to the OEFFE device. Loctite® 409 (Henkel, Mississauga, Canada) was used to seal the adapters to the device and allowed to cure for 1 h. Any openings, holes, or extra spaces were filled with Loctite® to prevent leaks. A Nikon 7000 digital camera was mounted on a tripod and was used to record images.

The electrolyte was prepared with 25 mM 4-(2-hydroxyethyl)-1-piperazineethanesulfonic acid (HEPES) (99.5%) and was adjusted with 10 M NaOH to pH 7.5. Triton X-100 (0.001 [w/v]) was added, and the mixture was deoxygenated by bubbling with N_2 overnight. The electrolyte was then used to prepare a sample solution of 250 mM fluorescein, rhodamine B, and rhodamine 6G each. All solutions were prepared using de-ionized H_2O.

The hydrodynamic flow of the electrolyte was driven by a continuous flow syringe pump system (New Era Pump System Inc, Farmingdale, NY, USA). The electrolyte flow rates in the experiment highlighted in the paper was 5.00 ± 0.05 mL/min. A separate syringe pump (Harvard Apparatus Pump II, Saint-Laurent, Canada) was used to introduce the sample at a flow rate of 4.00 ± 0.01 μL/min. Experiments were carried out at room temperature (22^{o}C). The OEFFE device was placed on top of metal blocks, which were in contact with ice packs, to help prevent overheating.

Before using the device, it was placed into the oven over night at 65^{o}C. This was to ensure that the plastic was not wet. The wet surface caused the device to swell and clog the channels. The OEFFE device was allowed to cool to room temperature after removal from the oven. A 10% EtOH solution was passed through the device to wet the entire surface prior to the electrolyte. The electrolyte was then introduced along with the sample at the prescribed flow rates mentioned above. The voltage applied to the system was 500 V, which represents an electric field strength of 50.0 V/cm inside the separation channel. For 12 hours, the current was recorded and digital pictures were taken to monitor the sample separation quality in the presence of an electric field. Bubbles were successfully detached from the surface of the electrodes, but we added an occasional mechanical shock to the chimneys to aid in detachment. After the device was used, it was flushed with de-ionized H_2O to wash out any remaining electrolyte and placed back in the oven to dry overnight at 65^{o}C.

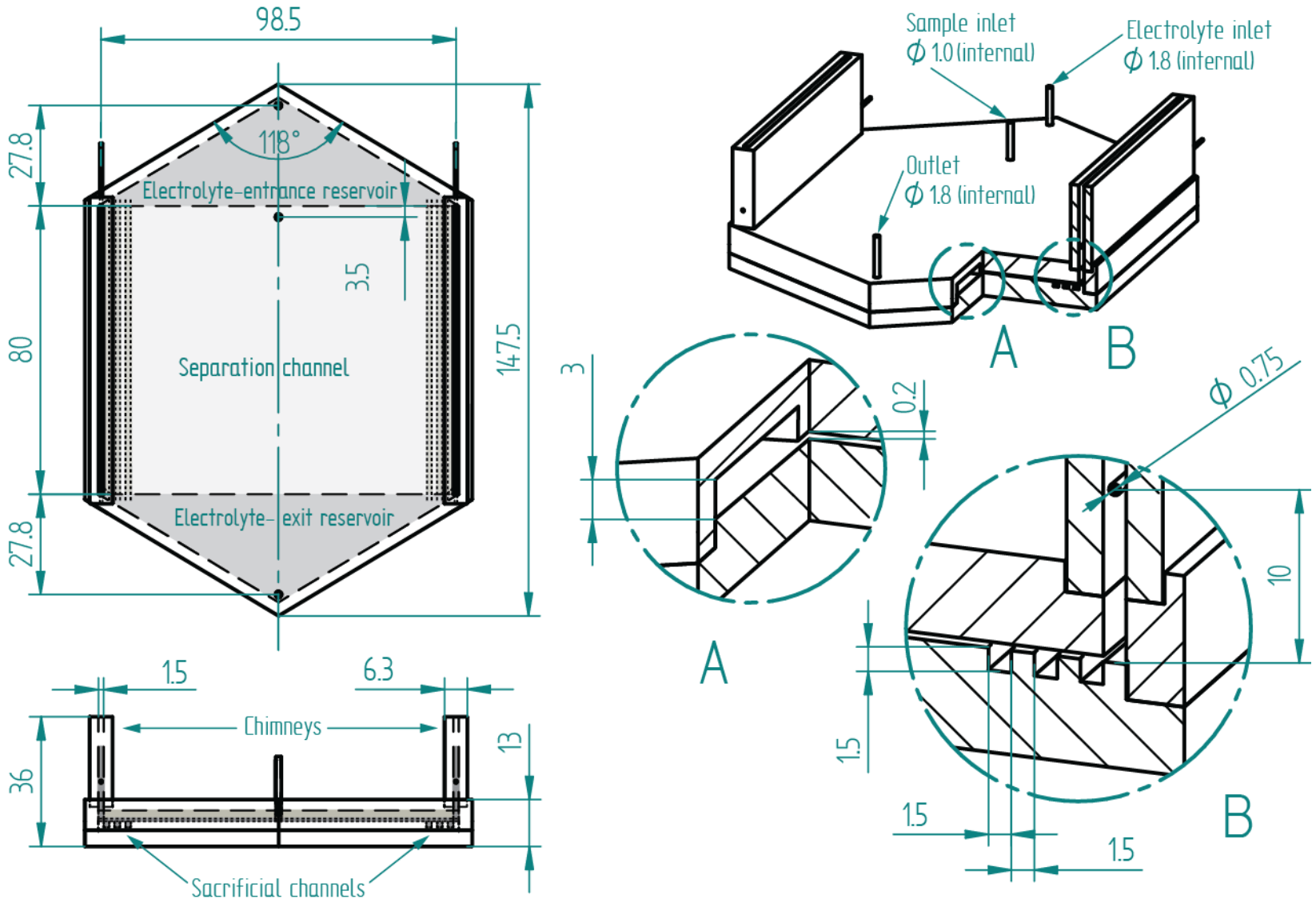

Figure S1. Schematic representation of an assembled OEFFE device. All units are in mm. This model differs from that illustrated in **Fig. 1d** by omitting sample outlets in the separation channel. The purpose of this communication was to demonstrate successful bubble removal, and steady-state continuous electrophoretic purification. Therefore, for simplicity of the experiment, we used a common output for electrolyte and products.

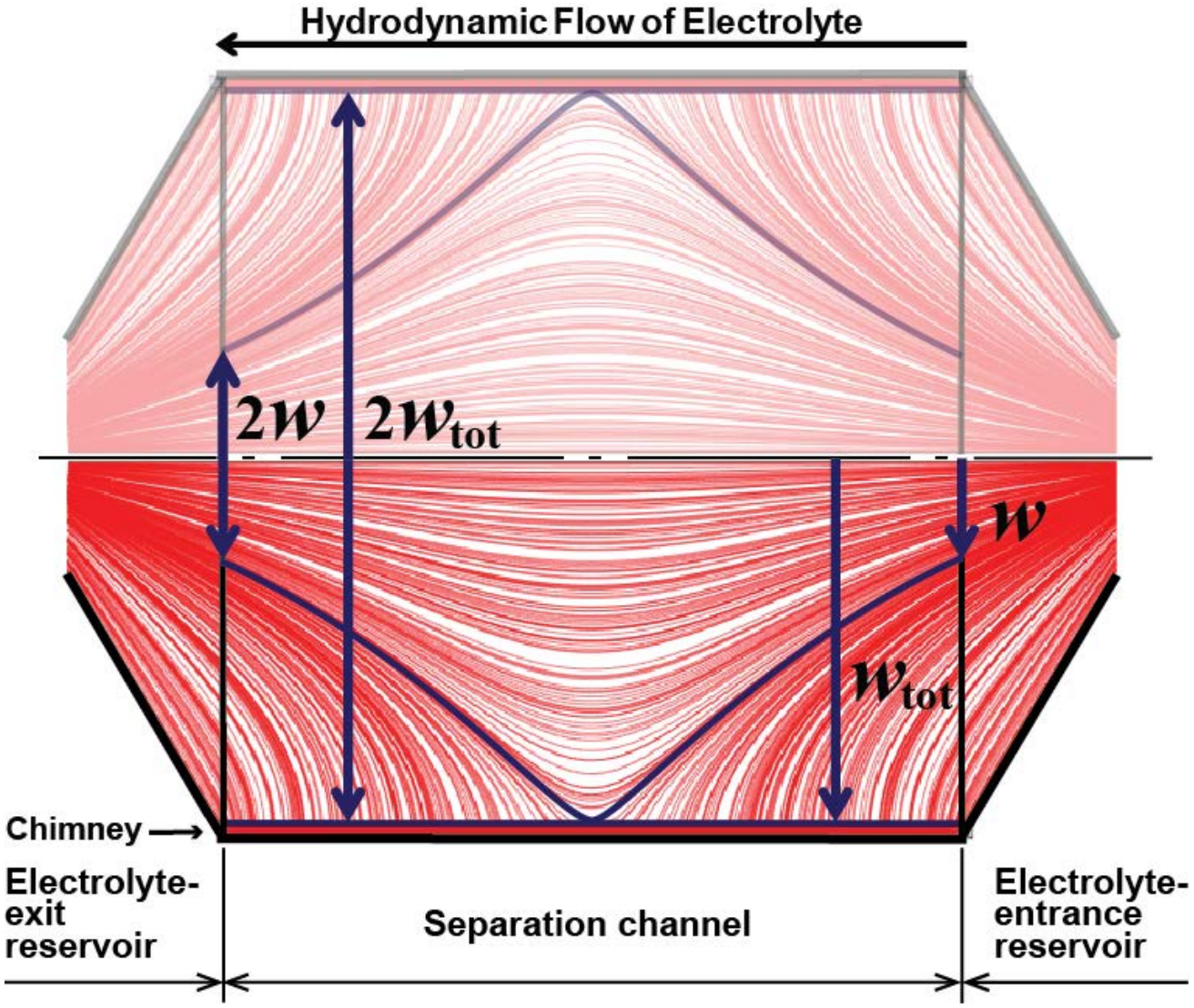

Figure S2. Top-view in-silico COMSOL simulation of hydrodynamic flow trajectories in the presence of chimneys. For conceptual clarity, we illustrate the entire virtual device. The symmetry plane is present at half of the width (w_{tot}), and for simulation performance, calculating the hydrodynamic flow streamlines is less time-consuming. The semi-transparent half of the virtual device is the mirror image of that shown in the lower half with respect to geometric features and simulated streamlines. Thus, the optimization parameter (w/w_{tot}), in this case, is equal to that calculated for the entire virtual device ($2w/2w_{tot}$).

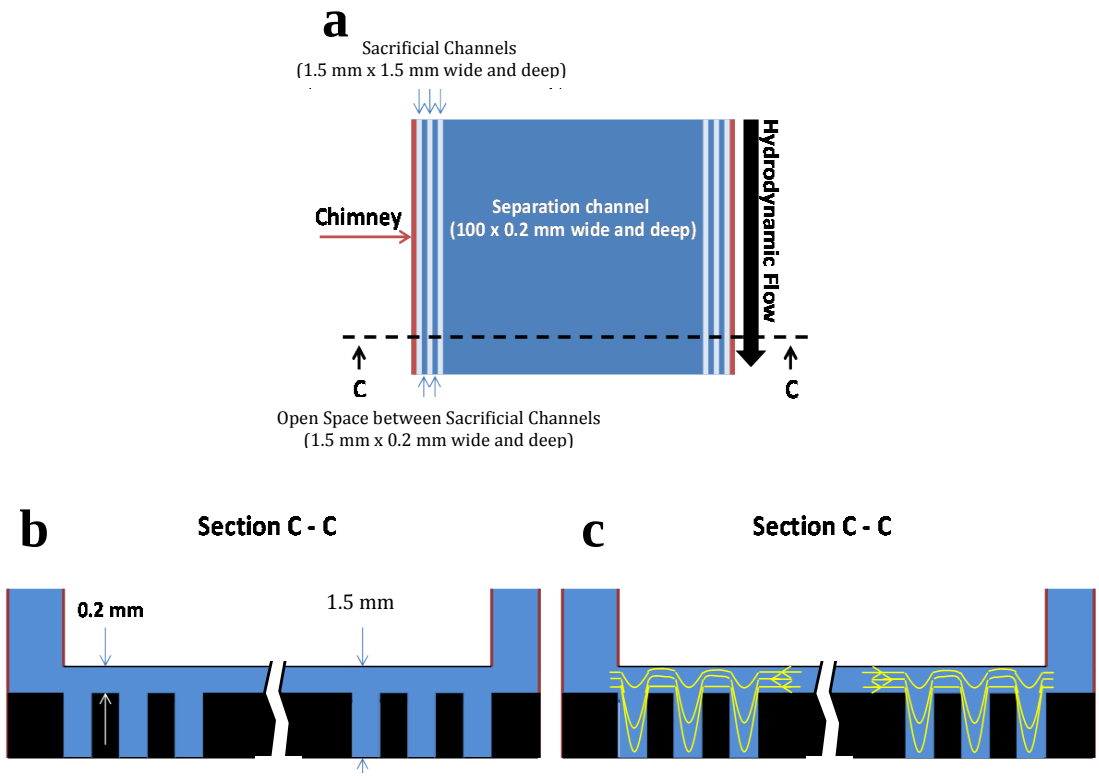

Figure S3. Schematic representation of (**a**) a planar separation channel and its cross section (C-C) to illustrate (**b**) the positioning of the sacrificial channels, and (**c**) liquid streamlines flowing tangentially to the hydrodynamic flow. The yellow streamlines project the necessary trajectories for liquid to flow from the separation channel into the chimneys. The sacrificial channel profile in (**c**) illustrates two major considerations that can contribute to limiting hydrodynamic flow into the chimneys. First, the fluid flow profile in these channels, particularly the shallow (200 µm) space between the sacrificial channels, is laminar. Such shallowness of channels suggests that shear forces should dominate fluid exchange between sacrificial channels. As a result, the viscosity of water would inhibit the possibility of changing velocity abruptly (as shown by the yellow streamlines), and move across three sacrificial channels and into the chimneys. Second, due to the increased volumetric flow rate of the fluid in the deeper sacrificial channels, and the corresponding increase in the effect of inertial forces on fluid flow, it is less likely for the fluid to diverge from its original straightforward trajectories (in sacrificial channels) and enter chimneys.The planar view and cross section are not to scale.

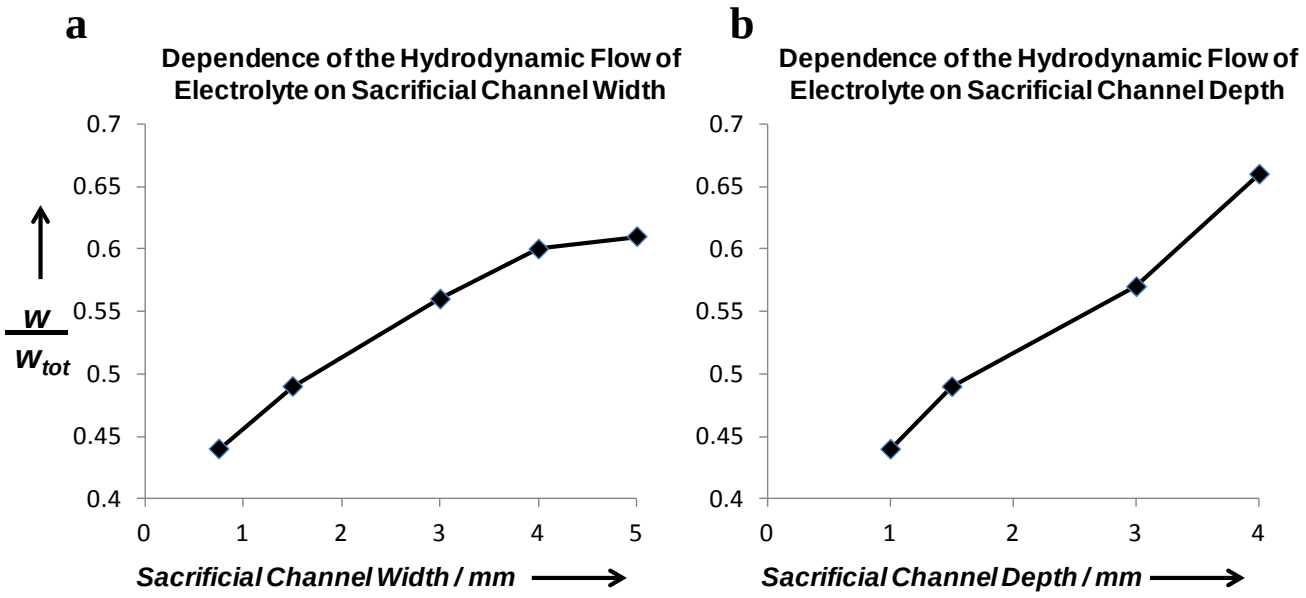

Figure S4. The dependence of the hydrodynamic flow uniformity on sacrificial channel dimension. (a) The width is varied when the sacrificial channel depth is set at 1.5 mm. (b) The depth is varied when the sacrificial channel width is set at 1.5 mm. Increasing the depth of the sacrificial channel had the greatest effect, however due to the tools we had available to us, we were limited to a sacrificial channel depth of 1.5 mm. With respect to the width of the sacrificial channel, larger widths provide improvement in flow uniformity. However, we chose a width of (1.5 mm) because it was prudent to consider adding further sacrificial channels before using very wide channels that would occupy more space in the separation channel. The ultimate purpose of the sacrificial channels was to improve flow uniformity by exploiting the combination of shear forces in shallow (0.200 mm) channels and inertial forces in the deeper (1.5 mm) sacrificial channels. For this, we need to use more than one sacrificial channel.

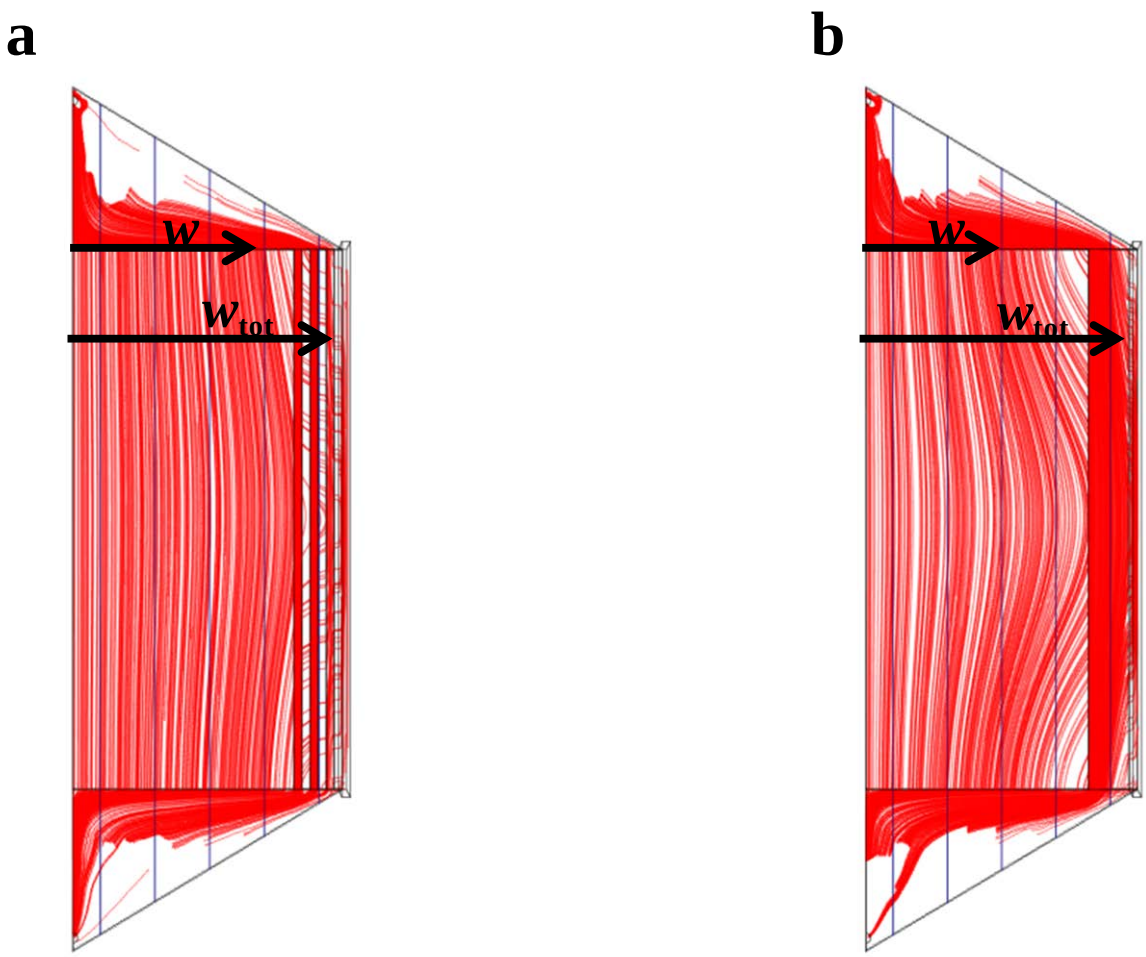

Figure S5. In-silico optimization of electrolyte flow in OEFFE by comparison of one wide sacrificial channel vs. three narrow sacrificial channels. (**a**) The presence of 3 narrow sacrificial channels decreases the divergence in flow compared with (**b**) where only 1 wide sacrificial channel is used. This is corroborated by the w/w_{tot} values of 0.69 and 0.56 for (**a**) and (**b**) respectively. This validates the greater significance of multiple sacrificial channels compared with one wide sacrificial channel.

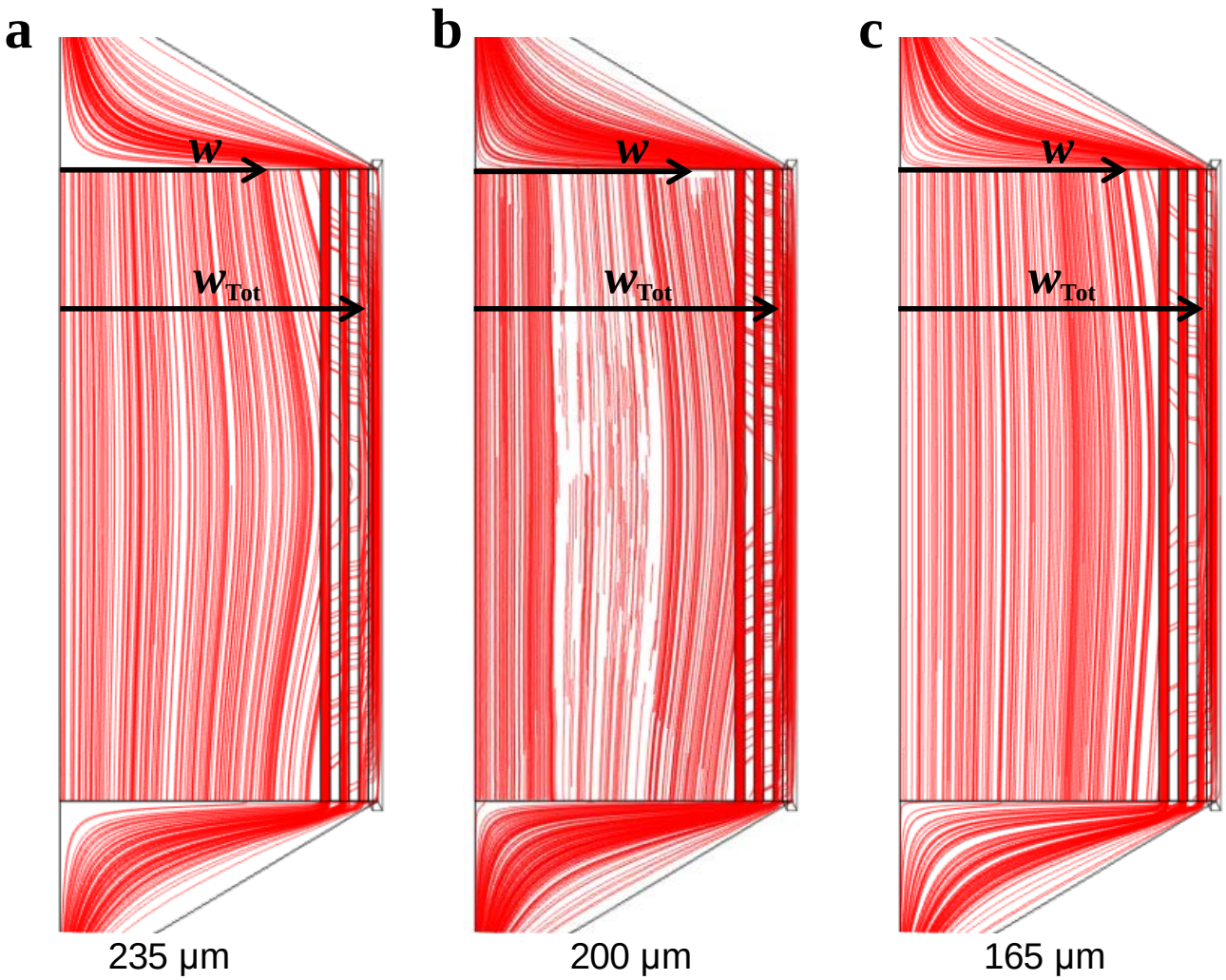

Figure S6. In-silico validation of OEFFE robustness with respect to separation channel depth. The w/w_{tot} values are 0.68, 0.69, and 0.71 for the (**a**) 235 µm, (**b**) 200µm, (**c**) 165 µm deep separation channels respectively. Both panels (**a**) and (**c**) illustrate two possible depths, which reflect the precision of machining when fabricating a 200 µm separation channel. The w/w_{tot} values suggest negligible influence on flow non uniformity.

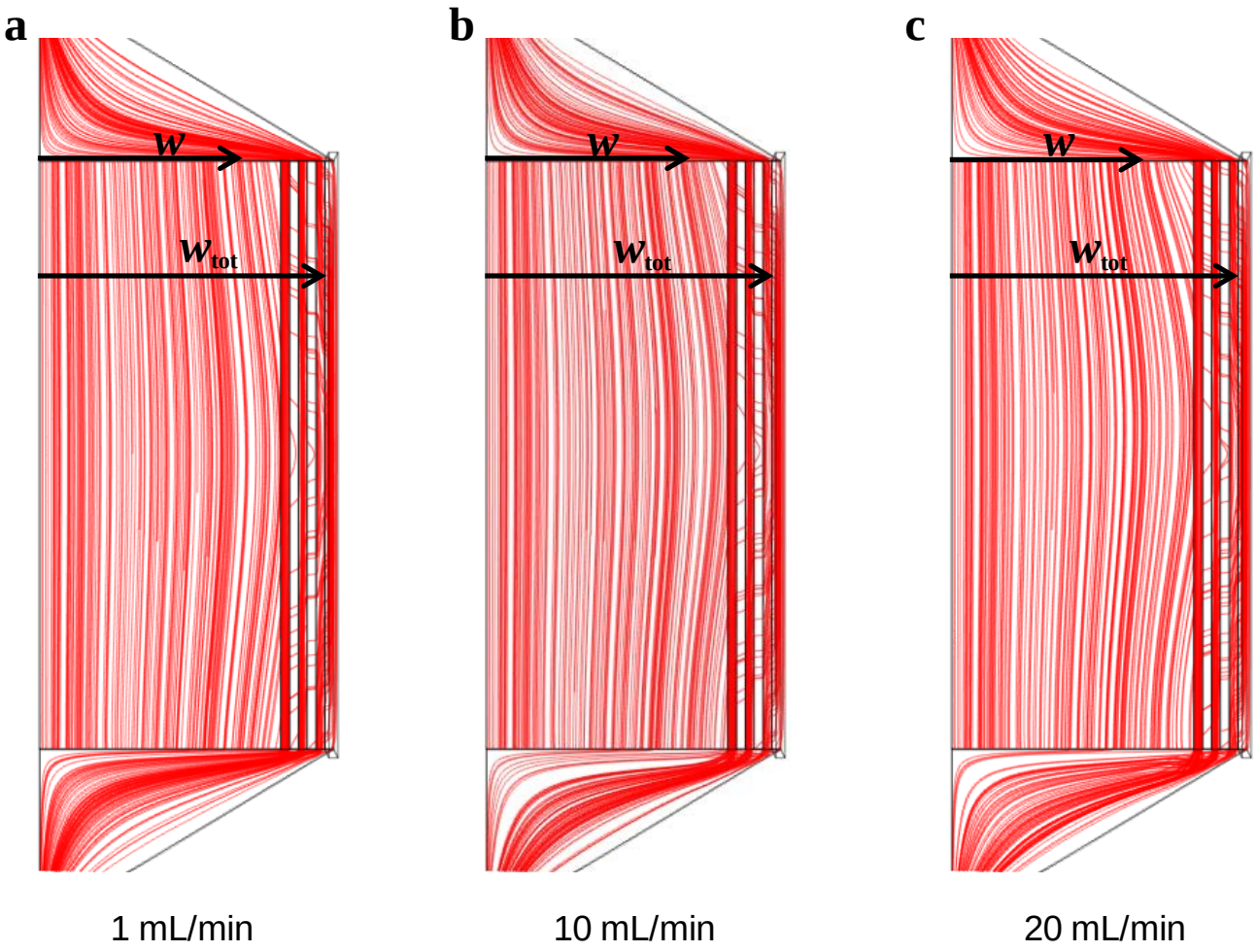

Figure S7. In-silico validation of OEFFE robustness with respect to hydrodynamic flow rate. Variations in hydrodynamic flow rates were varied from (**a**) 1 mL/min to (**b**) 10 mL/min, and (**c**) 20 mL/min to evaluate if w/w_{tot} would change drastically. In effect, all simulations demonstrate that the w/w_{tot} value is consistent across these three flow rates (w/w_{tot} = 0.69).The tested flow rate range is well beyond the flow rate error of the syringe pumps used (± 1%). It was not logical, however, to expand the flow rate range further because higher flow rates would decrease resolution, and slower flow rates would increase band broadening. Both situations would result in a decrease of separation quality.